Organic Electronics 15 (2014) 3546–3551

Contents lists available at ScienceDirect

Organic Electronics

journal homepage: www.elsevier.com/locate/orgel

Circuital modelling of S-shape removal in the current–voltage characteristic of TiO_x inverted organic solar cells through white-light soaking

B. Romero [a,*], G. Del Pozo [a], E. Destouesse [b], S. Chambon [b], B. Arredondo [a]

[a] Escuela Superior de Ciencias Experimentales y Tecnología, Universidad Rey Juan Carlos, C/Tulipán s/n, 28933 Móstoles, Madrid, Spain
[b] Univ. Bordeaux, IMS, UMR 5218, F-33400 Talence, France

ARTICLE INFO

Article history:
Received 12 May 2014
Received in revised form 1 July 2014
Accepted 20 September 2014
Available online 18 October 2014

Keywords:
Circuit modelling
Organic solar cell
S-shape
White-light activation
TiO_x

ABSTRACT

In this work light activation phenomenon in inverted bulk heterojunction (BHJ) organic solar cells (OSC) has been electrically modelled with a two-diode equivalent circuit. OSC are based on poly(3-hexylthiophene) (P3HT): 1-(3-methoxycarbonyl)-propyl-1-1-phenyl-(6,6) C61 (PCBM) with a titanium oxide (TiO_x) sublayer. Current–voltage (*I–V*) characteristics show a highly pronounced S-shape that is gradually removed during light activation process. The circuit used to model *I–V* curves includes two diodes in forward and reverse bias together with two parallel resistances, R_{P1} and R_{P2}. The parallel of the reverse bias diode and its corresponding resistance R_{P2} models the electrical behaviour of the TiO_x interlayer. This interlayer has been thermally treated at different temperatures, from 80 °C up to 180 °C, reducing the activation time from 400 s for unbaked devices down to 30 s for devices annealed at temperatures higher than 80 °C. The S-shape shown in the *I–V* characteristic is completely removed after a few minutes of white-light illumination. *I–V* curves recorded during the activation process have been fitted with the analytical solution of the two-diode circuit based on W-Lambert function. A decrease of the subcircuit 2 equivalent resistance has been found to be the cause of S-shape removal. This resistance diminishing is in good agreement with the increase of TiO_x conductance with baking temperature and white-light exposure time found by other authors.

1. Introduction

Solution-processed organic solar cells (OSC) have been rapidly developed in the last years due to the unique advantages they offer over their inorganic counterparts: low-cost and low temperature fabrication techniques, wide-area scalability, flexibility, thinness and lightweight [1]. Currently, OSC based on blends of conjugated polymer as donor materials blended with fullerene derivatives as electron acceptor material have become one of the most popular due to the high efficiencies achieved ~8% [2,3].

These organic devices often show the so-called S-shape, or kink, in the current–voltage (*I–V*) characteristic [4,5]. This feature usually appears in the fourth quadrant, and drastically reduces fill factor (FF) and therefore device efficiency (η). The origin of S-shape is still not clear. Several authors attribute this phenomenon to different causes such as dipoles defects at the interface [5], imbalance of charge carrier mobilities [6], and surface recombination rate of the cathode [7]. All these phenomena result in carrier accumulation inside the device [8], and thus in a change of the electric field distribution. This S-shape has been found both in direct and inverted solar cells [5] and in devices containing layers of different oxides, such as ZnO [9] and TiO_x [10]. While the origin of S-shape in ZnO OSC is commonly

* Corresponding author. Tel.: +34 914887178; fax: +34 914887049.
E-mail address: beatriz.romero@urjc.es (B. Romero).

http://dx.doi.org/10.1016/j.orgel.2014.09.033
1566-1199/

attributed to adsorbed molecular oxygen acting as electron trap [11], the origin of S-shape in TiO_x cells is still not clear. Some authors also attribute it to adsorbed O_2 [12] while others attribute it to shallow traps located between TiO_x valence and conduction bands [13]. Whatever its origin is, some studies point out that S-shape can be removed by means of post processing treatments such as thermal annealing in direct solar cells [14] or UV light exposure in inverted ones [11,15,16]. These treatments induce trap filling, which increases TiO_x conductivity and thus removes S-shape [17].

Although the physics underneath of conduction mechanisms in organic and inorganic devices are quite different, *I–V* characteristics can be modelled using similar circuits. Therefore the standard circuital models traditionally used for inorganic devices are also valid for organic ones [18]. Standard *I–V* curves of OSC are usually modelled by a simple one diode circuit model (Fig. 1a) that consists of a constant current source that models photogenerated current in parallel with a diode that models dark current. Two parasitic resistances, series and shunt resistance, are usually needed to take into account contact layers and leakage currents respectively. Other authors use more complicated circuits to model standard *I–V* behaviour [19]. However, all these models are not valid for S-shaped *I–V* characteristic since they do not reproduce the curvature change. In order to model S-shape different models have been proposed in literature. Mazhari [20] proposed a three-diode model that was able to generate the kink in the *I–V* curves (Fig. 1b). Araujo de Castro et al. proposed a two-diode circuit to simulate the kink of MEH-PPVC60 solar cells (Fig. 1c). The second diode, in reverse bias operation, is the responsible of S-shape and, according to the authors, it takes into account the effect of traps at the interface [21]. The same authors solved numerically this model making some approximations. This two-diode circuit was analytically solved by means of W-Lambert function without approximations [22]. A modified version of this circuit (Fig. 1d), including a third diode was proposed by García-Sánchez et al. in order to describe the exponential-like upward bend observed at large voltages [23].

In this work we have used the modified two diode circuit proposed by Araujo de Castro to model experimental *I–V* data of inverted OSC based on P3HT:PCBM. Among all models mentioned above, this one has been chosen since it is the simplest one that simulates accurately S-shape. In addition, the TiO_x interlayer has already been associated to a counter diode in similar structures [24]. A thin layer of TiO_x was deposited on top of ITO substrate and used as electron selective layer (ESL). The final device structure was ITO/TiO_x/P3HT:PCBM/MoO_3/Ag. The TiO_x layer was annealed at different temperatures, from 80 °C to 180 °C prior deposition of the active layer. During white light illumination, the *I–V* curve evolves and the initial S-shape is completely removed after a few minutes of exposure. *I–V* curves recorded during the activation process every 4 s have been fitted with the exact analytical expression of the two-diode model (Fig. 1c) in order to study the evolution of the circuital parameters with the white-light exposure time. As it will be presented, the removal of S-shape is related to a simultaneous increase of diode 2 inverse saturation current together with a decrease of the parallel resistance of subcircuit 2. Both trends diminish the total equivalent resistance of subcircuit 2, which indicates an increase of the TiO_x conductivity, improving carrier extraction and ultimately removing S-shape.

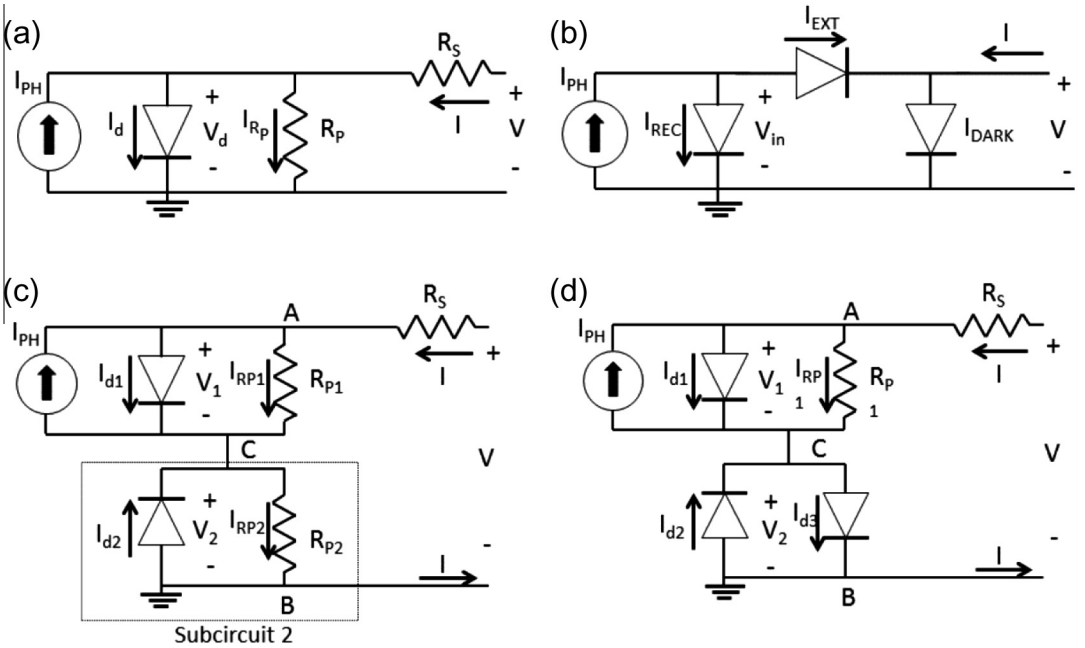

Fig. 1. (a) Standard circuit model for standard *I–V* characteristics, (b) model proposed by Mazhari to simulate S-shape [20], (c) model proposed by Araujo de Castro [21] to simulated S-shape [21] and (d) model proposed by García-Sánchez to simulate S-shape and upward bend at high voltages [23].

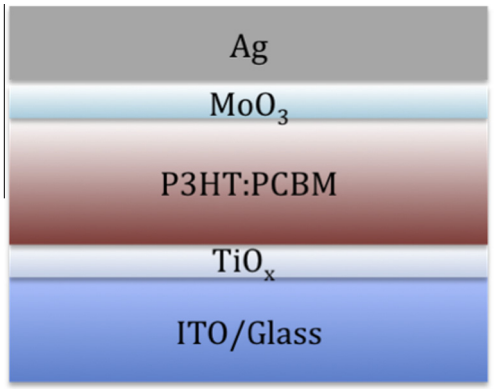

Fig. 2. Device layer structure: ITO/TiO_x/P3HT:PCBM/MoO_3/Ag.

2. Experimental details

Fig. 2 shows the structure of the seven fabricated devices. The only difference among devices was the annealing temperature of TiO_x: 80 °C, 100 °C, 120 °C, 140 °C, 160 °C and 180 °C prior deposition of the active layer. A sample without thermal treatment was also used for the sake of comparison. Devices were characterized using a K.H.S. Solar Celltest-575 solar simulator (Metal-Halide source) with AM1.5 G filters set to 100 mW/cm^2 with a calibrated radiometer (IK 1400BL). Labview controlled Keithley 2400 SMU enabled the measurement of *I–V* curves every 4 s to study the evolution of the *I–V* curve during white-light illumination. A complete description of the fabrication and characterization process can be found in [17].

3. Results and discussion

3.1. Circuit model and mathematical procedure

The circuit model used to simulate the S-shape in *I–V* curves is shown in Fig. 1c. This circuit model, proposed by Araujo de Castro et al. [21], consists of two subcircuits: the main one, subcircuit 1, is the traditional circuit used for standard *I–V* curves. The second one, subcircuit 2, is connected in series with the main one and is responsible of the S-shape. When the total equivalent resistance associated to subcircuit 2 becomes negligible, *I–V* curves recover the standard shape. According to the authors, subcircuit 2 models the effect of traps at the interface between active layer and cathode. In our particular case, subcircuit 2 models the electrical behaviour of TiO_x interlayer between active layer and the cathode (ITO). In the two limiting cases, diode 2 can be reduced to an open or a short circuit, and the modified circuit becomes the standard one in both situations. When diode 2 behaves as an open circuit, the total series resistance equals to $R_S + R_{P2}$. In this case the TiO_x interlayer acts as an insulator. On the other hand, when diode 2 behaves as a short circuit, it bypasses R_{P2} and total series resistance equals R_S. This second case is associated to a high TiO_x conductance. The intermediate cases between these two limiting situations result in the appearance of the S-shape.

In [22] the circuit of Fig. 1c was analytically solved using the Lambert W-function without approximations. The exact expression relating current and voltage is given by:

$$\begin{aligned} V = {} & (I + I_{PH} + I_{01})R_{P1} \\ & - \frac{n_1 kT}{q} W\left\{ \frac{q}{n_1 kT} I_{01} R_{P1} \exp\left[\frac{q}{n_1 kT} R_{P1}(I + I_{PH} + I_{01}) \right] \right\} \\ & + \frac{n_2 kT}{q} W\left\{ \frac{q}{n_2 kT} I_{02} R_{P2} \exp\left[\frac{q}{n_2 kT} R_{P2}(I - I_{02}) \right] \right\} \\ & + (I - I_{02})R_{P2} + IR_S \end{aligned} \tag{1}$$

where I_{01} and I_{02} are saturation currents and n_1 and n_2 are the ideality factors for diodes 1 and 2 respectively, q is the elementary charge, k is the Boltzmann constant, and T the absolute temperature. I_{PH} stands for the photogenerated current, R_{P1} and R_{P2} are the parallel resistances of forward diode 1 and reverse diode 2 respectively and R_S stands for the series resistance.

The fitting procedure of Eq. (1) to the experimental data has been performed using a minimum squared routine in Matlab. Although Eq. (1) sets voltage as a function of current, the fit has been done in the voltage domain in order to avoid numerical problems in the constant current region, where small current variations lead to great voltage changes.

3.2. Results

The white-light irradiation treatment completely removes S-shape on each sample after several minutes. Therefore the last curve recorded of each device does not show the kink and thus it has been fitted in the first place with the standard traditional model using as fitting parameters I_{01}, n_1, R_{P1}, I_{PH} and R_S. These parameters are shown in Table 1.

As it can be observed in the table, saturation current ranges between 0.6×10^{-7} A and 6.6×10^{-7} A, and ideality factor ranges between 2.1 and 2.8. Photogenerated current ranges between 0.76 mA and 1 mA, having its maximum at 120 °C baking temperature. R_{P1} is the most varying parameter, it ranges between 8 kΩ and 7.4 MΩ. However, in all the curves R_{P1} is high enough to not consider leakage current as a limiting factor in *I–V* characteristics. In fact, the

Table 1
Circuit parameters of the last *I–V* curve showing no kink after activation with white-light for all fabricated devices.

Annealing temperature	I_{01} (A)	n_1	R_{P1} (kΩ)	R_S (Ω)	I_{PH} (A)
No annealing	1.9E−07	2.4	7.4×10^3	62	7.60E−04
80 °C	6.5E−07	2.7	8.04	53	7.71E−04
100 °C	0.6E−07	2.1	99	26	7.85E−04
120 °C	2.6E−07	2.5	76.1	18	1.00E−03
140 °C	1.7E−07	2.4	71.3	24	8.19E−04
160 °C	6.6E−07	2.8	5.39	17	8.73E−04
180 °C	2.2E−07	2.5	16	15	9.20E−04

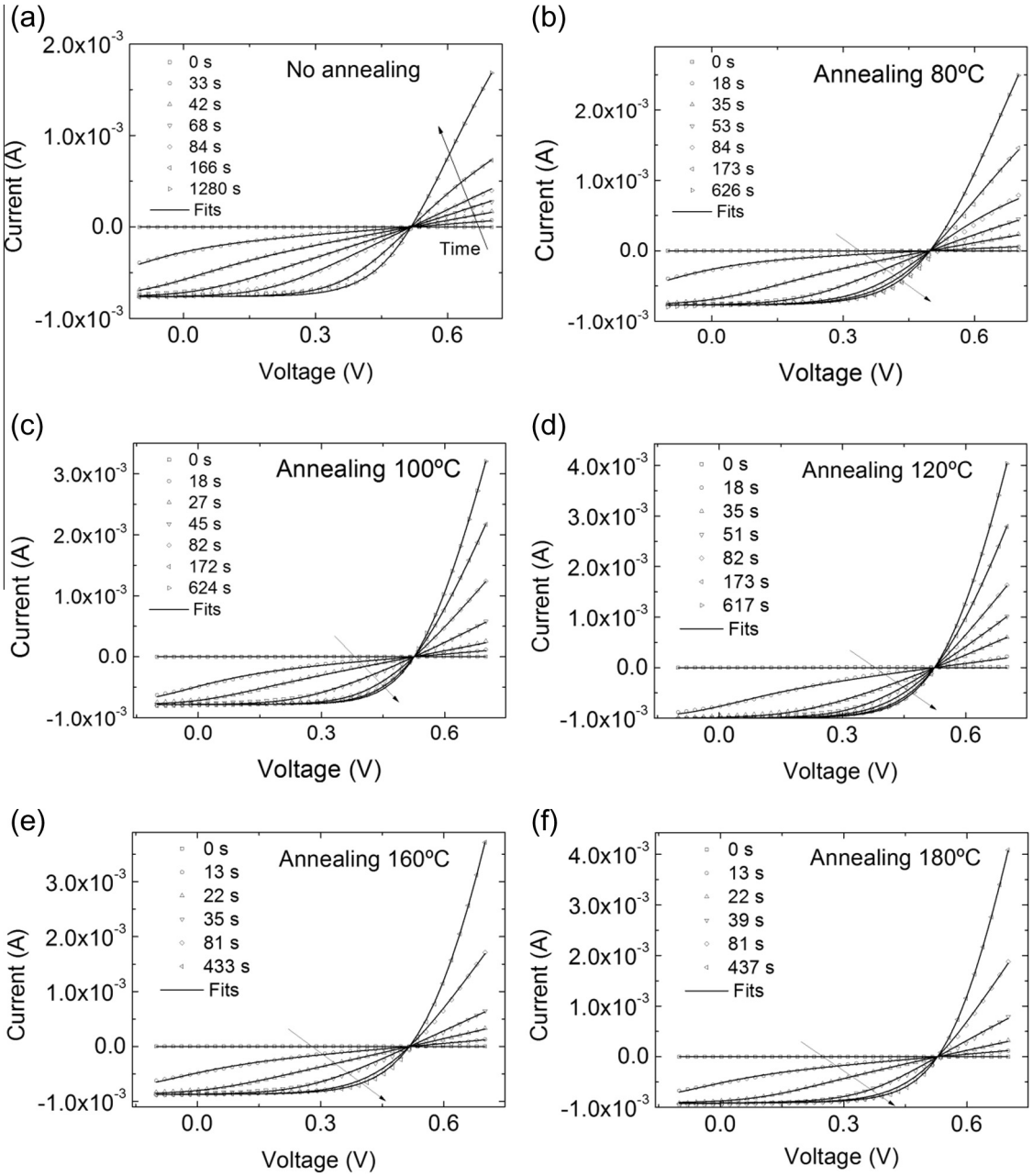

Fig. 3. Experimental (dots) and fits (solid lines) *I–V* characteristics recorded during the white-light illumination for devices with TiO_x interlayer baked at: (a) no baking, (b) 80 °C, (c) 100 °C, (d) 120 °C, (e) 160 °C and (f) 180 °C.

effect of R_{P1} can be neglected, as the curves are flat at zero bias. As it can be observed in Table 1, R_S has a decreasing trend with baking temperature ranging from 62 Ω for unbaked devices, to 15 Ω for devices annealed at 180 °C. This result indicates that R_S is somehow linked to the insulating nature of TiO_x interlayer, which decreases with baking temperature, thus reducing R_S. These results are in good agreement with those obtained in [17] for TiO_x conductivity. Authors measured TiO_x conductance for devices with different TiO_x baking temperatures and showed that conductivity increases more that one order of magnitude when TiO_x interlayer was baked at temperatures higher than 80 °C.

When fitting the curves showing S-shape, the values corresponding to subcircuit 1 (except R_S) have been fixed to those shown in Table 1. The *I–V* curves of each sample have been fitted using as parameters I_{02} and R_{P2}. Subcircuit 2 can play the role of R_S since it can model both contacts resistance and the resistance presented by TiO_x. Therefore, in order to reduce fitting parameters R_S has been set to

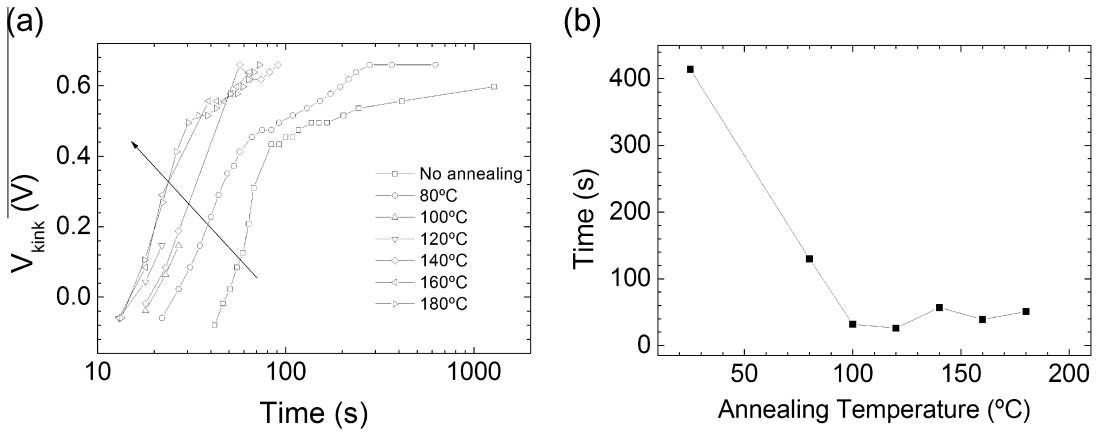

Fig. 4. (a) V_{kink} vs white-light illumination time for fabricated devices and (b) time needed to remove S-shape vs baking temperature.

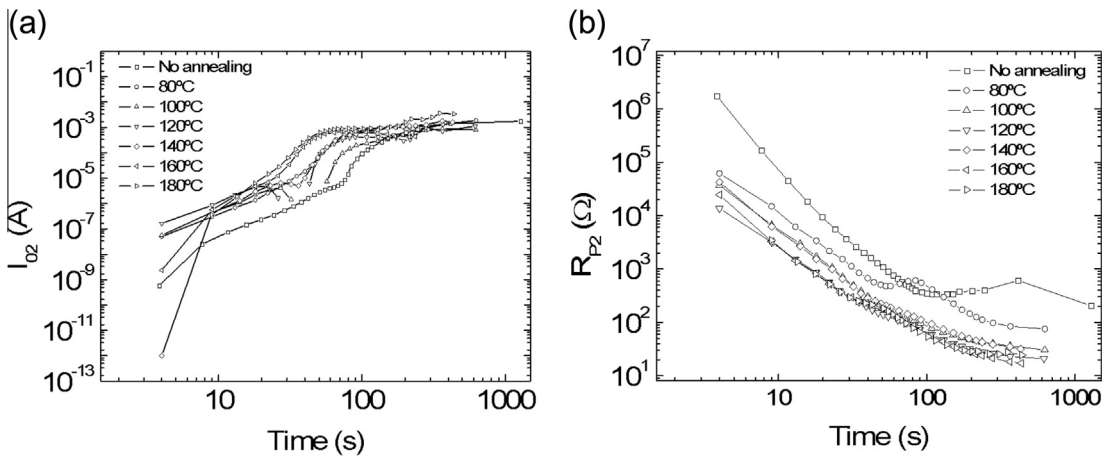

Fig. 5. Inverse saturation current (a) and parallel resistance (b) of subcircuit 2 vs white-light illumination time for the seven fabricated devices.

zero. Ideality factor of subcircuit 2 has been fixed to $n_2 = 4$. This value has been chosen after verifying that it leads to the best fits in terms of smallest total error.

Fig. 3 shows experimental data (symbols) and fits (solid lines) of the *I–V* curves recorded during the light activation process for the different samples. The figure shows that S-shape is completely removed in all the samples after a few minutes of white-light exposure. As it can also be observed, as the annealing temperature of the TiO_x layer increases, the white-light exposure time required to remove S-shape decreases.

Most of the *I–V* curves in Fig. 3 show S-shape, thus they present an inflection point in the fourth quadrant at kink voltage (V_{kink}). Kink voltage is defined as the voltage at which the curve turns from concave to convex, and it is mathematically defined as the voltage at which the second derivative of current with respect to voltage equals zero. When $V_{kink} > V_{OC}$, S-shape disappears in the fourth quadrant indicating that S-shape is no longer affecting FF or efficiency. As the irradiation time increases so does the voltage at which the kink appears.

Fig. 4a shows V_{kink} vs irradiation time for all the fabricated devices. For all samples, V_{kink} shifts to higher values as irradiation time increases, in accordance with the disappearance of the S-shape. Interestingly, when the temperature of the TiO_x thermal treatment decreases, the increase of the V_{kink} is delayed. This can suggests that with lower annealing temperature of the TiO_x, the traps density in TiO_x is higher, leading to longer activation period to fully remove the S-shape. Fig. 4b shows the exposure time needed to completely remove the S-shape from the fourth quadrant. This time drastically decreases from 400 s to 30 s when the TiO_x layer is annealed at temperatures higher than 100 °C.

Fig. 5 shows the fitting parameters I_{02} and R_{P2} vs white-light illumination time for each sample. The trend of these parameters is the same for all the samples. I_{02} increases with irradiation time and saturates to 10^{-3} A approx around 100 s. On the other hand, R_{P2} decreases with irradiation time and also saturates to 20 Ω approx around 100 s. The simultaneous increase of I_{02} and decrease of R_{P2} results in a lowering of subcircuit 2 equivalent resistance that

ultimately reduces S-shape. This reduction of subcircuit 2 total resistance with exposure time indicates an improvement of TiO_x conductivity, which is in good agreement with results published in [10,17]. This improvement is more remarkable in devices with TiO_x baked at temperatures higher than 100 °C, due to a reduction of traps density with baking temperature.

4. Conclusions

A modified two-diode circuit has been used to simulate the evolution of S-shape with white-light soaking of P3HT:PCBM based OSC with a TiO_x interlayer baked at different temperatures from 80 °C up to 180 °C. The model includes a new subcircuit in series with the standard model that takes into account the insulating behaviour of the TiO_x interlayer, due to the presence of traps. Results show that S-shape is completely removed after several minutes of illumination in all the samples. This is attributed to a reduction of total equivalent resistance of subcircuit 2, indicating an increase of TiO_x conductance with white-light exposure time.

Acknowledgement

This work has been supported by Comunidad Autónoma de Madrid under Project S2009/ESP-1781.

References

[1] B. Azzopardi, C.J.M. Emmott, A. Urbina, F.C. Krebs, J. Mutale, J. Nelson, Economic assessment of solar electricity production from organic-based photovoltaics modules in a domestic environment, Energy Environ. Sci. 4 (2011) 3741–3753.
[2] Z.C. He, C.M. Zhong, X. Huang, W.Y. Wong, H.B. Wu, L.W. Chen, S.J. Su, Y. Cao, Simultaneous enhancement of open-circuit voltage, short-circuit current density, and fill factor in polymer solar cells, Adv. Mater. 23 (2011) 4636–4643.
[3] C.E. Small, S. Chen S, J. Subbiah, CM Amb, SW Tsang, TH Lai, JR Reynolds, F. So, High-efficiency inverted dithienogermole–thienopyrrolodione-based polymer solar cells, Nat. Photonics 6 (2012) 115–120.
[4] A. Wagenpfahl, D. Rauh, M. Binder, C. Deibel, V. Dyakonov, S-shaped current–voltage characteristics of organic solar devices, Phys. Rev. B 82 (2010) 115306-1–115306-8.
[5] A. Kumar, S. Sista, Y. Yang, Dipole induced anomalous S-shape *I–V* curves in polymer solar cells, J. Appl. Phys. 105 (2009) 094512-1–094512-6.
[6] W. Tress, A. Petrich, M. Hummert, M. Hein, K. Leo, M. Riede, Imbalanced mobilities causing S-shaped IV curves in planar heterojunction organic solar cells, Appl. Phys. Lett. 98 (2011) 063301-1–063301-3.
[7] B.Y. Finck, B.J. Schwartz, Understanding the origin of the S-curve in conjugated polymer/fullerene photovoltaics from drift-diffusion simulations, Appl. Phys. Lett. 103 (2013) 053306-1–053306-4.
[8] J.C. Wang, X.C. Ren, S.Q. Shi, C.W. Leung, P.K.L. Chan, Charge accumulation induced S-shape *J–V* curves in bilayer heterojunction organic solar cells, Org. Electron. 12 (2011) 880–885.
[9] T. Kuwabara, Y. Kawahara, T. Yamaguchi, K. Takahashi, Characterization of inverted-type organic solar cells with a ZnO layer as the electron collection electrode by ac impedance spectroscopy, ACS Appl. Mater. Interf. 1 (2009) 2107–2110.
[10] B. Ecker, H.J. Egelhaaf, R. Steim, J. Parisi, E. von Hauff, Understanding S-shaped current–voltage characteristics in organic solar cells containing a TiO_x interlayer with impedance spectroscopy and equivalent circuit analysis, J. Phys. Chem. C 116 (2012) 16333–16337.
[11] M.R. Lilliedal, A.J. Medford, M.V. Madsen, K. Norrman, F.C. Krebs, The effect of post-processing treatments on inflection points in current–voltage curves of roll-to-roll processed polymer photovoltaics, Sol. Energy Mater. Sol. Cells 94 (2010) 2018–2031.
[12] H. Schmidt, K. Zilberbert, S. Schmale, H. Flugge, T. Riedl, W. Kowalsky, Transient characteristics of inverted polymer solar cells using titanium oxide interlayers, Appl. Phys. Lett. 96 (2010) 243305-1–243305-3.
[13] C.S. Kim, S.S. Lee, E.D. Gómez, J.B. Kim, Y.-L. Loo, Transient photovoltaic behavior of air-stable, inverted organic solar cells with solution-processed electron transport layer, Appl. Phys. Lett. 94 (2009) 113302-1–113302-3.
[14] G. del Pozo, B. Romero, B. Arredondo, Evolution with annealing of solar cell parameters modelling the S-shape of the current–voltage characteristic, Sol. Energy Mater. Sol. Cells 104 (2012) 81–86.
[15] R. Steim, S.A. Choulis, P. Schilinsky, C.J. Brabec, Interface modification for highly efficient organic photovoltaics, Appl. Phys. Lett. 92 (2008) 093303-1–093303-3.
[16] T. Kuwabara, C. Iwata, T. Yamaguchi, K. Takahashi, Highly durable inverted-type organic solar cell using amorphous titanium oxide as electron collection electrode inserted between ITO and organic layer, Sol. Energy Mater. Sol. Cells 92 (2008) 1476–1482.
[17] S. Chambon, E. Destouesse, B. Pavageau, L. Hirsch, G. Wantz, Towards an understanding of light activation processes in titanium oxide based inverted organic solar cells, J. Appl. Phys. 112 (2012) 094503-1–094503-6.
[18] J.M. Nunzi, Organic photovoltaic materials and devices, C. R. Phys. 3 (2002) 523–542.
[19] A. Cheknane, H.S. Hilal, F. Djeffal, B. Benyoucef, J.P. Charles, An equivalent circuit approach to organic solar cell modelling, Microelectron. J. 39 (2008) 1173–1180.
[20] B. Mazhari, An improved solar cell circuit model for organic solar cells, Sol. Energy Mater. Sol. Cells 90 (2006) 1021–1033.
[21] F. Araujo, J. Heier, F. Nüesch, R. Haby, Origin of the kink in current–density versus voltage curves and efficiency enhancement of polymer-C60 heterojunction solar cells, IEEE J. Sel. Top. Quantum Electron. 16 (2010) 1690–1699.
[22] B. Romero, G. del Pozo, B. Arredondo, Exact analytical solution of a two diode circuit model for organic solar cells showing S-shape using Lambert W-functions, Sol. Energy 86 (2012) 3026–3029.
[23] F.J. García-Sánchez, D. Lugo-Muñóz, J. Mucci, A. Ortiz-Conde, Lumped parameter modelling of organic solar cells' S-Shaped *I–V* characteristics, IEEE J. Photovoltaics 3 (2013) 330–335.
[24] M. Glatthaar, M. Riede, N. Keegan, K. Sylverster-Hvid, B. Zimmermann, M. Niggemann, A. Hinsch, A. Gombert, Efficiency limiting factors of organic bulk heterojunction solar cells identified by electrical impedance spectroscopy, Sol. Energy Mater. Sol. Cells 91 (2007) 390–393.